European Radiology
EXPERIMENTAL
EUROPEAN SOCIETY OF RADIOLOGY

ORIGINAL ARTICLE

Open Access

Deep learning for predicting future lesion emergence in high-risk breast MRI screening: a feasibility study

Bianca Burger[1], Maria Bernathova[2], Philipp Seeböck[1], Christian F. Singer[3,4], Thomas H. Helbich[2] and Georg Langs[1,5*]

Abstract

Background International societies have issued guidelines for high-risk breast cancer (BC) screening, recommending contrast-enhanced magnetic resonance imaging (CE-MRI) of the breast as a supplemental diagnostic tool. In our study, we tested the applicability of deep learning-based anomaly detection to identify anomalous changes in negative breast CE-MRI screens associated with future lesion emergence.

Methods In this prospective study, we trained a generative adversarial network on dynamic CE-MRI of 33 high-risk women who participated in a screening program but did not develop BC. We defined an anomaly score as the deviation of an observed CE-MRI scan from the model of normal breast tissue variability. We evaluated the anomaly score's association with future lesion emergence on the level of local image patches (104,531 normal patches, 455 patches of future lesion location) and entire CE-MRI exams (21 normal, 20 with future lesion). Associations were analyzed by receiver operating characteristic (ROC) curves on the patch level and logistic regression on the examination level.

Results The local anomaly score on image patches was a good predictor for future lesion emergence (area under the ROC curve 0.804). An exam-level summary score was significantly associated with the emergence of lesions at any location at a later time point ($p = 0.045$).

Conclusions Breast cancer lesions are associated with anomalous appearance changes in breast CE-MRI occurring before the lesion emerges in high-risk women. These early image signatures are detectable and may be a basis for adjusting individual BC risk and personalized screening.

Relevance statement Anomalies in screening MRI preceding lesion emergence in women at high-risk of breast cancer may inform individualized screening and intervention strategies.

Key points

- Breast lesions are associated with preceding anomalies in CE-MRI of high-risk women.
- Deep learning-based anomaly detection can help to adjust risk assessment for future lesions.
- An appearance anomaly score may be used for adjusting screening interval times.

Keywords Breast cancer, High-risk women, Magnetic resonance imaging, Deep learning, Generative adversarial network

*Correspondence:
Georg Langs
georg.langs@meduniwien.ac.at
Full list of author information is available at the end of the article

Springer Open

Graphical Abstract

DL for predicting lesion emergence in high-risk breast MRI screening: a feasibility study

- Breast lesions are associated with preceding anomalies in CE-MRI of high-risk women.
- Deep learning-based anomaly detection can help to adjust risk assessment for future lesions.
- An appearance anomaly score may be used for adjusting screening interval times.

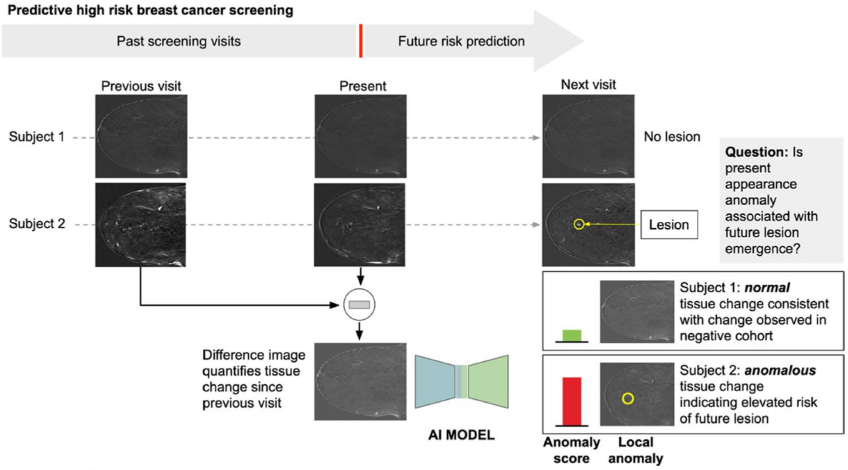
Predictive high risk breast cancer screening
Past screening visits
Future risk prediction
Previous visit
Present
Next visit
Subject 1
Subject 2
No lesion
Lesion
Question: Is present appearance anomaly associated with future lesion emergence?
Difference image quantifies tissue change since previous visit
AI MODEL
Subject 1: *normal* tissue change consistent with change observed in negative cohort
Subject 2: *anomalous* tissue change indicating elevated risk of future lesion
Anomaly score
Local anomaly

A deep learning model detects anomalies in the appearance change of breast CE-MRIs between screening visits. An elevated anomaly score in negative scans (BI-RADS 1) predicts emergence of lesions in future screening scans.

MRI anomalies preceding lesion emergence in high-risk women may inform individualized screening

Burger B et al (2023) Eur Radiol Exp. DOI: 10.1186/s41747-023-00343-y

Background

Up to 20% of BCs occur in women with a genetic predisposition [1]. To achieve a significant risk reduction, these women may opt for a prophylactic bilateral mastectomy or are offered intensified annual screening [2, 3]. Although mammography is sufficient in some women [4], international societies have issued guidelines for high-risk BC screening, recommending contrast-enhanced magnetic resonance imaging (CE-MRI) of the breast as a supplemental diagnostic tool due to its high sensitivity [5–7]. Given limited resources, the effectiveness and feasibility of screening programs depend on the balance between early detection capability and over-screening.

Clinical risk models rely on static categorical variables including patient demographics, personal and family history, and risk factors driven by the patient's age [8], resulting in the inclusion of women into rigid screening regimes. Although CE-MRI improves screening sensitivity significantly, cases of invasive BC can be missed, or cancer can develop between screens as interval BC [9, 10]. In hindsight, about a third of cancers detected in high-risk screening programs had been already visible at the last negative CE-MRI screen, indicating missed cancers by reporting radiologists despite improved training [11–13]. This points to the opportunity to exploit even negative screening CE-MRI exams for risk assessment enabling dynamic screening regimes.

Here, deep learning (DL) models may detect precursor image signatures in CE-MRI associated with an increased risk of future lesion emergence. Image-based individual short- to mid-term risk adjustment and corresponding optimization of screening intervals could enable continual personalization of screening programs leading to improved screening effectiveness [14–17].

DL has been widely implemented in healthcare for pattern recognition, including radiology [18, 19]. In breast imaging, DL systems have been quickly evolving, surpassing the performance and clinical value of traditional computer-aided detection systems for mammography [20] or dynamic CE-MRI [21]. Supervised models detect lesions [22] by either parsing imaging data [23] or analyzing entire MRI slices at once [24, 25]. Furthermore, DL may reduce workload by being trained to triage negative screens [26, 27], which would allow radiologists to concentrate only on suspicious scans. DL-based prediction models have also been proposed to predict treatment response or assess the overall risk of cancer [28–30]. In the context of breast cancer, initial results using mammography of women at normal risk suggest the feasibility to predict certain pathological conditions in the future [14–16]. However, to our knowledge, dynamic risk assessment based on CE-MRI of high-risk women has not been explored yet.

In this study, we investigated two questions: (1) Can DL models detect "anomalies" as deviations from normal tissue changes in negative CE-MRI screens of the breast of high-risk women? (2) Are these automatically detected deviations to which we refer to as anomalies associated with future lesion emergence?

Methods

Study overview

The ratio of positive to negative cases in screening cohorts is low, and the precursor signatures of lesions are not known. For an automated approach to dynamic risk profiling the negative cohort could therefore serve as a training cohort to create a model that becomes sensitive to deviations from normal variability in new cases and identifies them as anomalies. To answer our research questions, we therefore first built a model capturing the variability of breast tissue in healthy women between screening visits. New CE-MRI examinations were then assessed by comparing their appearance with the normal appearance model. Deviations from the model of normal variability were thereby captured by an anomaly score (Fig. 1). Since the detected anomalies might serve as a basis for dynamic risk profiling, their association with future lesions was evaluated.

Data collection

This study on prospectively collected data was approved by our institutional ethics committee. We analyzed anonymized patient data of subjects who gave informed consent for inclusion. We collected longitudinal dynamic CE-MRI scans of the breast from 1,119 high-risk women with a lifetime risk for breast cancer higher than 20%, who underwent high-risk screening at our institution from 2002 to 2019. Studies of women with unilateral or bilateral mastectomy or with implant reconstruction were excluded. Subjects whose studies were acquired exclusively until 2007 were also excluded. 2007 was chosen as the cutoff due to a scanner switch becoming

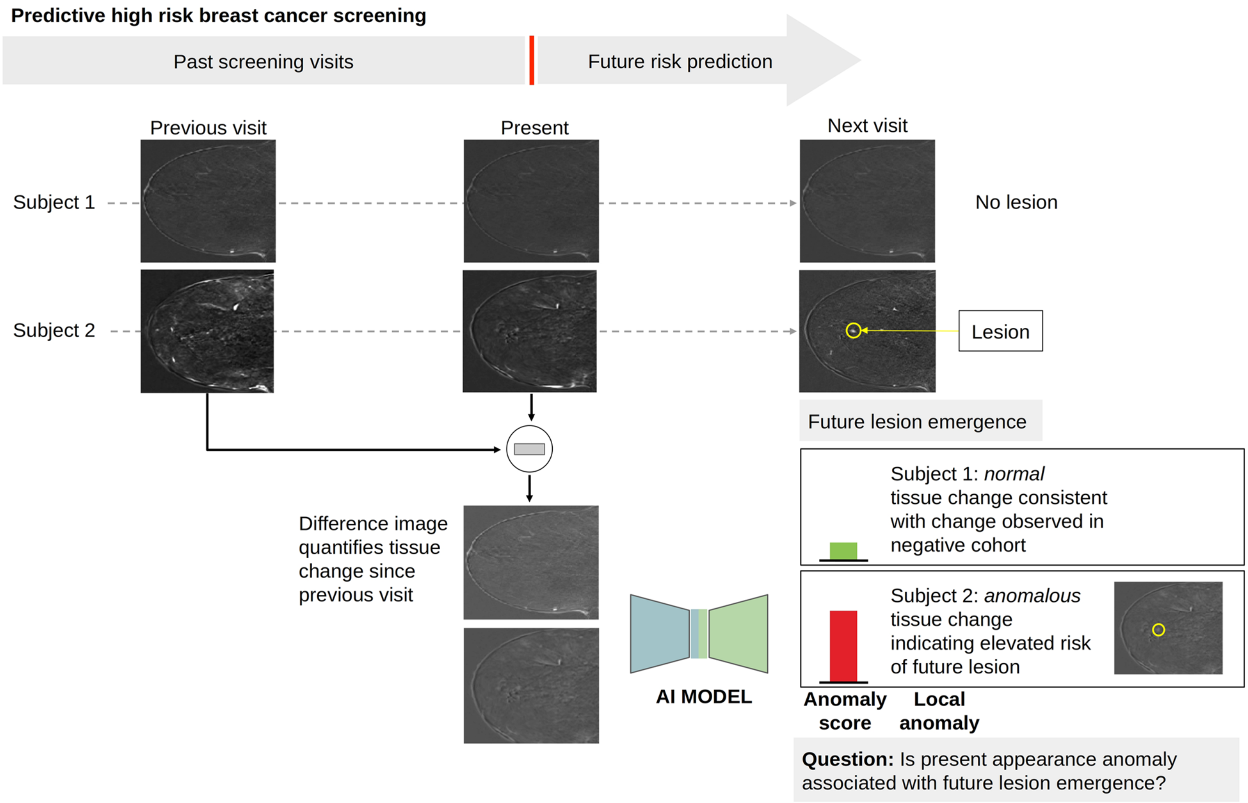
Predictive high risk breast cancer screening
Past screening visits
Future risk prediction
Previous visit
Present
Next visit
Subject 1
Subject 2
No lesion
Lesion
Future lesion emergence
Difference image quantifies tissue change since previous visit
AI MODEL
Subject 1: *normal* tissue change consistent with change observed in negative cohort
Subject 2: *anomalous* tissue change indicating elevated risk of future lesion
Anomaly score
Local anomaly
Question: Is present appearance anomaly associated with future lesion emergence?

Fig. 1 Study overview for identifying anomalies in screening CE-MRI of the breast associated with future lesions. A deep learning model detects anomalies in the appearance change of breast CE-MRIs between screening visits. An elevated anomaly score in negative scans (BI-RADS 1) predicts the emergence of lesions in future screening scans. Anomalies may serve as a basis for dynamic risk profiling in breast cancer screening to optimize individual screening intervals. *BI-RADS* Breast Imaging and Reporting Data System, *CE-MRI* Contrast-enhanced magnetic resonance imaging

effective at the beginning of 2008. We identified subjects for whom at least three imaging exams were available, of which the first two were BI-RADS 1. This resulted in a set of 96 subjects, 63 subjects with three BI-RADS 1 exams forming the negative cohort, and 23 subjects with two BI-RADS 1 exams and a subsequent BI-RADS 2, 3, 4, or 5 exams forming the positive cohort. BI-RADS 2 and 3 lesions were also included in the positive cohort since we were interested in differentiating normal tissue from any type of lesion.

We conducted preprocessing, including intra-patient registration, breast segmentation, and patch extraction (more details in the "Preprocessing" section and Supplementary Material). Subjects with unsatisfactory registration or segmentation results or a breast size too small to extract patches of the desired size were excluded. The final dataset therefore comprised 44 women in the negative cohort and 20 women in the positive cohort. Figure 2 gives an overview of the creation of our dataset.

MRI acquisition

During the study period, two scanners and corresponding protocols were in use. We only summarize the most important information for this study. A more detailed description of imaging protocols can be found in Riedl et al. [31, 32] and Milos et al. [33]. From 2002 to 2007 (Period 1), scans were performed with a 1.0-T scanner (Gyroscan T10-NT, Philips, Amsterdam, the Netherlands). T1-weighted three-dimensional gradient-echo dynamic sequences were obtained once before and 6 times after the injection of a single dose of a gadolinium-based contrast agent (Dotarem (gadoteric acid) 0.1 mmL/kg, rate 3 mL/s with 20 mL saline flash) at intervals of 70 s. For each image, 30–36 axial slices with a spacing between slices of 4.0–4.5 mm and a matrix of 256 × 256 (1.25–1.48 mm isotropic) were done. From 2008 to 2019, a 1.5-T MRI scanner Magnetom Avanto (Siemens, Berlin, Germany) was used. From 2008 to 2013 (Period 2), T1-weighted dynamic sequences were

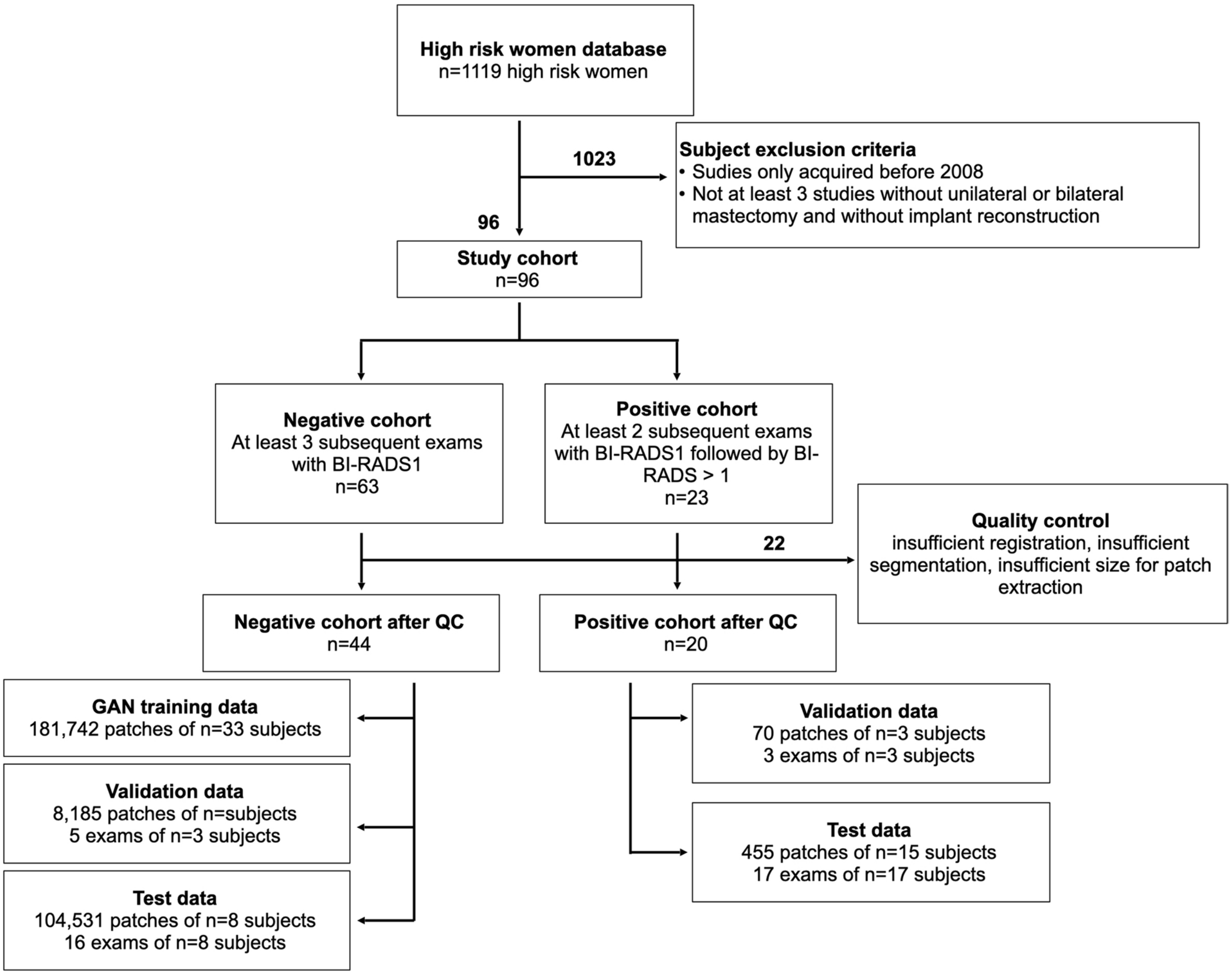
High risk women database
n=1119 high risk women
1023
Subject exclusion criteria
• Sudies only acquired before 2008
• Not at least 3 studies without unilateral or bilateral mastectomy and without implant reconstruction
96
Study cohort
n=96
Negative cohort
At least 3 subsequent exams with BI-RADS1
n=63
Positive cohort
At least 2 subsequent exams with BI-RADS1 followed by BI-RADS > 1
n=23
22
Quality control
insufficient registration, insufficient segmentation, insufficient size for patch extraction
Negative cohort after QC
n=44
Positive cohort after QC
n=20
GAN training data
181,742 patches of n=33 subjects
Validation data
8,185 patches of n=subjects
5 exams of n=3 subjects
Test data
104,531 patches of n=8 subjects
16 exams of n=8 subjects
Validation data
70 patches of n=3 subjects
3 exams of n=3 subjects
Test data
455 patches of n=15 subjects
17 exams of n=17 subjects

Fig. 2 Overview of dataset collection and use

acquired once before and four times after the injection of the contrast agent at intervals of 90 s. For each image, 48–54 axial slices with a spacing between slices of 3.30–3.85 mm and a matrix of 384 × 384 (0.91–0.99 mm isotropic) were done. From 2014 onwards (Period 3), the imaging protocol was updated and the axial dynamics were changed to a higher spatial resolution, Dixon fat-suppressed VIBE (volumetric interpolated breath-hold examination) sequence measured once before and three times after contrast agent injection at intervals of 90 s. From 80 to 88 axial slices with spacing between slices of 2.00 mm and a matrix of 512 × 512 (0.70–0.74 mm isotropic) were acquired.

Data preparation

The negative cohort was randomly split into a training (75%), validation (7%), and test set (18%), while the positive cohort was randomly split into a validation (15%) and test set (85%). There was no overlap of patients between sets. The training set consisted of MRI data of 33 women of the negative cohort from which 181,742 patches covering breast tissue were randomly extracted (more details on patch extraction in the "Preprocessing" section and Supplementary Material). The validation set was formed of 3 women from the negative cohort and 3 from the positive cohort, with corresponding randomly sampled 8,185 normal patches and 70 patches from locations with future lesions. The test set consisted of 104,531 randomly sampled normal patches extracted from 8 subjects in the negative cohort, and 455 randomly sampled patches extracted from locations with future lesions from 15 subjects in the positive cohort. The randomly extracted patches of the validation and test set were used to evaluate our anomaly detection approach locally. Two subjects were not part of the local evaluation on patch level because patches extracted from the location of the future lesion also contained more than 50 pixels of background and were therefore excluded.

To extract patches from locations with future lesions, the position was annotated by an expert radiologist with 25 years of experience in breast MRI but without specific training for this study, based on the first contrast-enhanced subtracted image of the visit for which the presence of the lesion was confirmed for the first time. ITK-Snap 3.8.0 was used for annotation (www.itksnap.org [34]). After intra-subject registration of visits, this manual annotation was also available for earlier examinations. See also Fig. 2 for an overview of the dataset creation.

In addition to local evaluation on the patch level, we also performed an examination-level evaluation, corresponding to a check of the entire MRI scan of a subject for a specific screening visit. For this, we applied our model to the subjects of validation and test set in a sliding window approach over the entire breast tissue. The sliding window approach was applied to all inter-visit difference images of consecutive BI-RADS 1-graded [35] visits available for a subject. As some subjects of the negative cohort provided more than one examination for evaluation, this results in 21 examinations from 11 subjects. In the positive cohort, 20 examinations from 20 subjects were used.

Preprocessing

Preprocessing included automated registration of follow-ups to reach spatial correspondence over time, automated breast segmentation to localize breast tissue in the scans, and extraction of patches as input for anomaly detection by our DL model. 64 × 64 pixel-sized patches were extracted from voxel value difference images $I_{i,j}^{diff}=I_i^{sub}$—I_j^{sub} between screening visits i and j. I_i^{sub} is the first post-contrast subtracted volume of visit i and i refers to the i^{th} available visit of a subject ordered according to the acquisition date. The lesion annotations were used additionally to extract patches from locations of future lesions. The number of patches extracted from a subject depended on breast size, ranging from around 200 to over 70,000 for subjects of the negative cohort and 20–40 patches of future lesion locations per subject of the positive cohort. More details on registration, segmentation, and patch extraction are provided in the Supplementary Material.

Training a fast anomaly detection generative adversarial network (f-AnoGAN)

The extracted patches from $I_{i,j}^{diff}$ represent differences in voxel values of subsequent visits and therefore the change of breast tissue appearance across time. We used anomaly detection to identify abnormal changes as possible precursors of future lesions. An overview of the anomaly detection framework is presented in Fig. 3. The idea of anomaly detection is to create a baseline model that captures normal variability. Then, deviations from this model are detected as anomalies (Fig. 3a). To model the variability of normal tissue appearance change over time, we used an f-AnoGAN [36] trained on the training set consisting only of patches extracted from the negative cohort. The proposed approach builds upon preliminary work presented by Burger et al. [37], significantly extending it with respect to anomaly detection, examination-level anomaly scoring, and more patients used for training and evaluation.

The f-AnoGAN consists of a generator *G*, discriminator *D*, and encoder *E* and is trained in two steps (Fig. 3b). First, *G* is trained to generate samples following the distribution of the training set using a random noise vector $\mathbf{z}$ as input, whereas *D* is trained to assess how well the generator

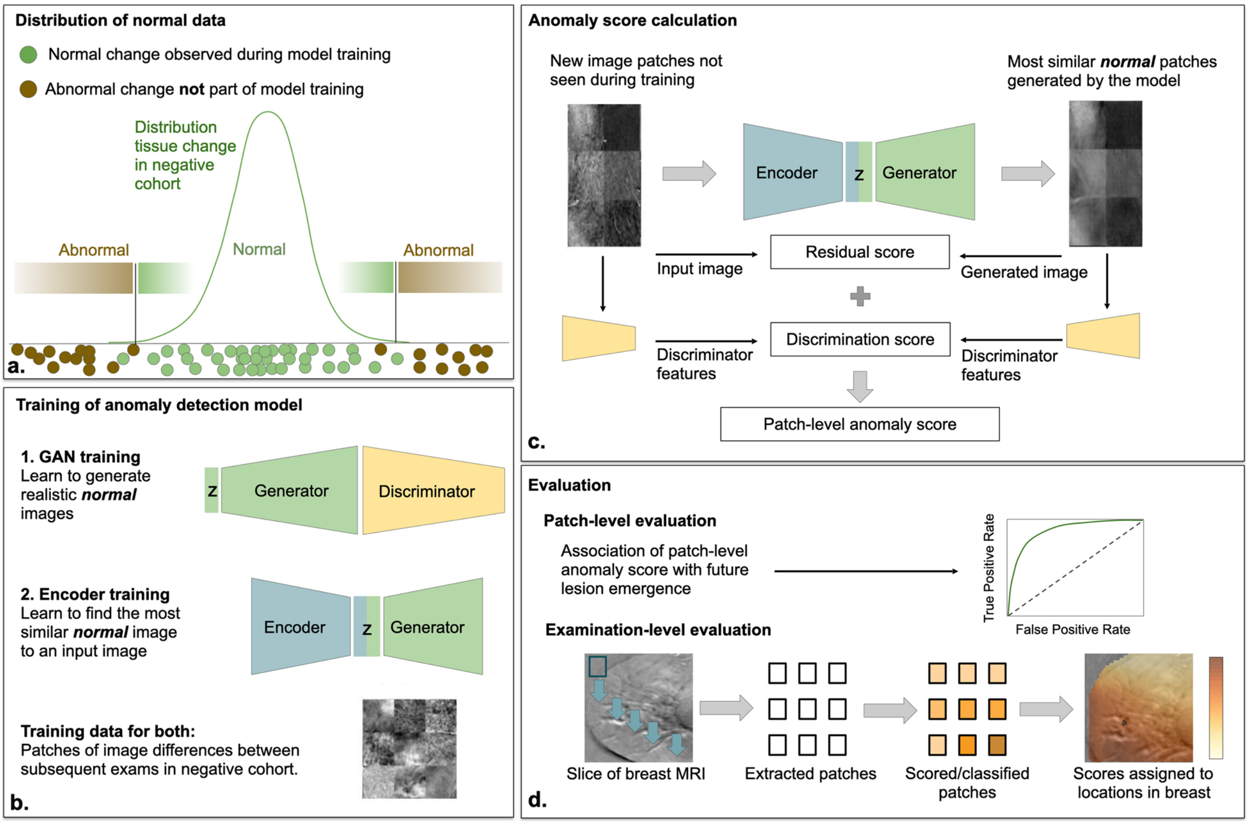
Distribution of normal data
● Normal change observed during model training
● Abnormal change **not** part of model training
Distribution tissue change in negative cohort
Abnormal
Normal
Abnormal
a.
Training of anomaly detection model
1. GAN training
Learn to generate realistic ***normal*** images
z
Generator
Discriminator
2. Encoder training
Learn to find the most similar ***normal*** image to an input image
Encoder
z
Generator
Training data for both:
Patches of image differences between subsequent exams in negative cohort.
b.
Anomaly score calculation
New image patches not seen during training
Most similar ***normal*** patches generated by the model
Encoder
z
Generator
Input image
Residual score
Generated image
Discriminator features
Discrimination score
Discriminator features
Patch-level anomaly score
c.
Evaluation
Patch-level evaluation
Association of patch-level anomaly score with future lesion emergence
True Positive Rate
False Positive Rate
Examination-level evaluation
Slice of breast MRI
Extracted patches
Scored/classified patches
Scores assigned to locations in breast
d.

Fig. 3 Overview of GAN-based anomaly detection and future lesion emergence prediction. **a** Tissue appearance change in negative follow-up CE-MRI scans of the breast that do not develop into breast cancer (normal data) forms a distribution in the space of different images that can be learned by a GAN model from normal cases. Anomalies are observations deviating from this distribution. **b** During training, a Generator *G*, a discriminator *D*, and an encoder *E* are trained on normal data. **c** During anomaly scoring a new image patch is processed by *E*, *G*, and *D*, resulting in an anomaly score. An anomaly score map for an entire CE-MRI volume is composed of anomaly scores evaluated in a sliding window across the entire volume. *CE-MRI* Contrast-enhanced magnetic resonance imaging, *GAN* Generative adversarial network

mimics the training data. Thereby the discriminator helps the generator to learn the training data distribution [38]. After training, G can synthesize examples that follow the distribution of normal tissue appearance change during follow-up exams. Second, the encoder E is trained to estimate the noise space embedding $\mathbf{z}$ of an input image $\mathbf{x}$. Finally, the trained models can be used to process a new input image $\mathbf{x}$ as follows: the encoder E maps x to the noise space representation $\mathbf{z}$, which is then used by G to generate a reconstructed image $\mathbf{y}=G(E(\mathbf{x}))$ which should be as similar as possible to $\mathbf{x}$. As f-AnoGAN is only trained on examples of normal variability, the generated image $\mathbf{y}$ is a normal version of the original image $\mathbf{x}$. If $\mathbf{x}$ shows normal variability itself, $\mathbf{x}$ and $\mathbf{y}$ will be very similar. If $\mathbf{x}$ shows an anomaly, $\mathbf{y}$ will be different from $\mathbf{x}$. This circumstance forms the basis of our anomaly detection strategy.

Calculating a local image anomaly score

The anomaly score measures the deviation from normal appearance change by comparing $\mathbf{x}$ and $\mathbf{y}$ and is based on two components: a residual score $L_R(\mathbf{x})$ and a discriminator score $L_D(\mathbf{x})$. The residual score measures the similarity of the original patch $\mathbf{x}$ and generated patch $\mathbf{y}$, whereas the discriminator score measures how normal the original patch $\mathbf{x}$ is. The anomaly score is calculated as a weighted sum $L(x)=L_R(\mathbf{x})+kL_D(\mathbf{x})$, where $k=0.1$ is a weighting term (Fig. 3c). Details on the calculation of $L_R(\mathbf{x})$ and $L_D(\mathbf{x})$ can be found in the Supplementary Material.

Evaluation of the local association between anomalies and future lesion emergence

For evaluating the association of the local anomaly score and the emergence of lesions in the future (Fig. 3d), we conducted bootstrapping [39] to obtain a distribution of receiver operating characteristic (ROC) curves on the test set. A single ROC curve was computed using 128 randomly selected patches from both the positive and negative cohort. This process was then repeated 10 times. ROC curves were chosen over precision-recall curves because we considered the correct classification of normal and abnormal changes equally important. Based on each single ROC curve, an optimal classification threshold was calculated using Youden's index [40]. Then, sensitivity, specificity, and false positive rate were calculated for this threshold. Finally, we computed 95% confidence intervals for these metrics. More details on performance evaluation are provided in the Supplementary Material.

Evaluation of an examination-level anomaly score

To get an examination-level score, we used a sliding window over the whole breast indicated by the segmentation mask (Fig. 3d) and aggregated over all voxels in both breasts. More details on how all local anomaly scores are aggregated into a single examination-level score can be found in the Supplementary Material. We evaluated the association between this examination-level score and the future occurrence of a lesion at any location by logistic regression, with the examination-level score as an independent and future lesion presence as the dependent variable. Additionally, a variable indicating the scanner type was included as an independent variable to control for possible correlations between scanner types and the anomaly score. To test for the statistical significance of the coefficient of the score, which corresponds to the significance of the association between examination-level score and future lesion, we used a Wald test with a significance level of $\alpha = 0.05$. We also provide performance measures and bootstrapping confidence intervals for various classification thresholds of the examination-level score T_{exam}. To additionally take the malignancy of future lesions into account, we also evaluated the model on BI-RADS 1, 2 *versus* BI-RADS 3, 4, and 5 classifications. The number of corresponding examinations are then 33 and 8, respectively. We decided to summarize BI-RADS 3 together with BI-RADS 4 and 5 lesions into one group to not further decrease the smaller class to 6.

Results

Anomalies predict future local lesion emergence

We evaluated the association of an elevated anomaly score with future lesion emergence at known future lesion locations using a distribution of ROC curves and obtained a confidence interval for the area under the ROC curve of (0.80, 0.82). The ROC curves are illustrated in Fig. 4a. The calculated optimal classification threshold for the anomaly score based on each ROC curve ranged from 552.43 to 603.88; 95% confidence intervals for true positive rate (sensitivity) and false positive rate at the determined cutoffs were 69 to 71% and 14 to 18%, respectively, and 82 to 86% for mean specificity. Table 1 shows the classification threshold,

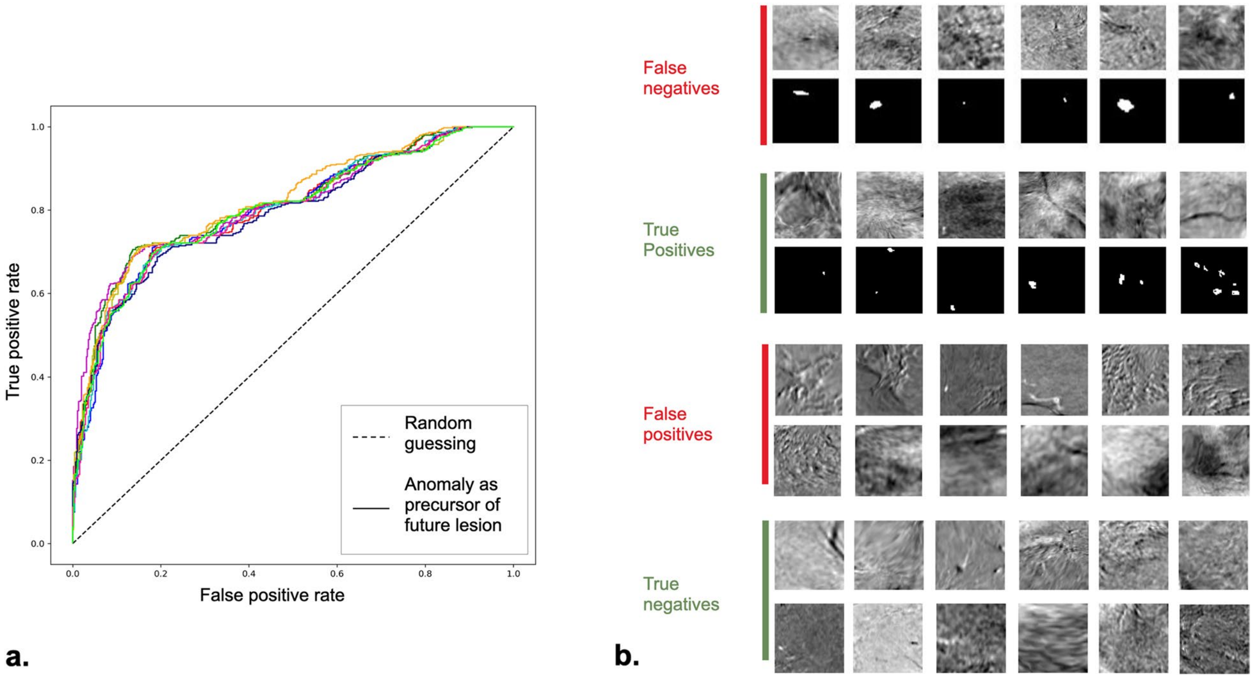

Fig. 4 The association of anomaly scores in negative scans (BI-RADS 1) and the emergence of lesions (BI-RADS 2 and above) in future scans. **a** ROC curves for 10 randomly drawn subsamples of the test set with equal numbers of subjects from the positive and negative cohorts are shown in different colors. Each color corresponds to one of the subsamples. **b** Illustrative examples of false negatives (low anomaly, future lesion), true positives (high anomaly, future lesion), false positives (high anomaly, no future lesion), and true negatives (low anomaly, no future lesion) in the test set. *BI-RADS* Breast Imaging and Reporting Data System

Table 1 Evaluation measures for a local association of anomaly score and future lesion occurrence

ROC curve number	AUC	Classification threshold based on ROC curve	Sensitivity	Specificity	False positive rate
1	0.81	585.14	70%	85%	0.15
2	0.80	552.43	71%	83%	0.17
3	0.82	585.14	70%	84%	0.16
4	0.81	572.91	70%	86%	0.14
5	0.81	559.86	71%	84%	0.16
6	0.82	595.71	69%	86%	0.14
7	0.81	585.14	70%	84%	0.16
8	0.80	595.71	69%	85%	0.15
9	0.80	559.86	71%	82%	0.18
10	0.82	552.43	71%	84%	0.16

ROC Receiver operating characteristic, *AUC* Area under the curve

sensitivity, false positive rate, specificity, and area under the curve for each ROC curve. Figure 4b shows examples of false positives and false negatives from the test set.

At the lesion level, for 5 future lesions out of 18, less than 50% of the patches covering the future lesion location were detected as anomalous. All these five lesions were benign, and four of the five had been classified as BI-RADS 2 when discovered by a radiologist. The fifth lesion had been classified as BI-RADS 4 when discovered by a radiologist but was later identified as mastitis.

An elevated examination-level score is associated with future lesion emergence at any breast location

To evaluate the association of the examination-level anomaly score with the emergence of future lesions through logistic regression we used the subjects from the validation and test set. Figure 5a shows the mean and standard deviation of examination-level scores corresponding to the mean over classified breast tissue voxels for examinations of subjects from the positive and negative cohort. The score lies by definition between 0 and 1. When predicting the emergence of a lesion from the examination-level score via logistic regression, the score's coefficient was found to be significantly different from 0 (coefficient = 2.006, 95% confidence interval 0.057 to 4.913; $p = 0.045$).

When investigating the association of the score with future lesion emergence, we also found hints for an association between score and acquisition period. More precisely, there was an association between images acquired in Period 1 and a high examination-level score as seen in Fig. 5b. At an examination-level classification threshold T_{exam} ranging from 0.1 to 0.9 most false positives corresponded to inter-subject difference images calculated based on at least one study acquired in Period 1 (yellow dots in Fig. 5b). Since we included a scanner variable in the logistic regression model, results, nevertheless, showed that the score is a significant independent predictor of future lesion emergence. Supplementary Table 1 summarizes several performance measures for various values of T_{exam}, yielding a good compromise at $T_{exam} = 0.7$ and $T_{exam} = 0.9$. When classifying BI-RADS 1, 2 *versus* BI-RADS 3, 4, and 5 with $T_{exam} = 0.7$, sensitivity and negative predictive value increase from 65 and 67% to 88% and 95%; however, specificity and positive predictive value drop from 67 and 65% to 61% and 38%.

Discussion

Our study shows that anomalous change of CE-MRI between negative screens is associated with future lesion emergence in high-risk women. Anomalies can be detected by a generative adversarial network (GAN) model trained on CE-MRI screens of women who remain BI-RADS 1 throughout the observation period. We evaluated the method on a large high-risk screening study cohort, achieving a mean area under the curve (AUC) of 0.804 in predicting future lesion emergence based on the current local anomaly score in negative CE-MRI screens. The score predicts a transition from BI-RADS 1 to BI-RADS 2, 3, 4, or 5 at a later time point. Additionally, we evaluated if the summary of anomaly scores in the entire breast is associated with future lesion emergence at any location and observed a significant association ($p = 0.045$).

This suggests that anomaly detection approaches may serve as a basis for dynamic risk scoring. In the context of high-risk screening, anomalies with an elevated risk of future lesion emergence could be used to adjust screening intervals, or as a support for radiologists assessing a screening scan. The paper forms a basis for future

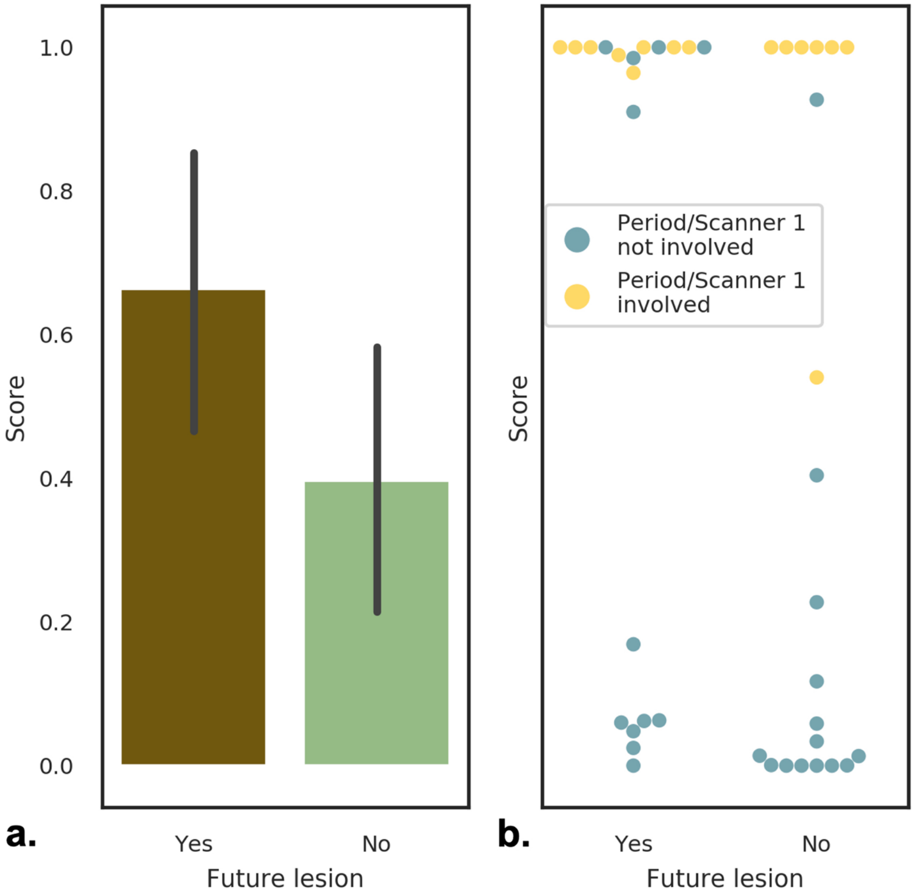

Fig. 5 Examination-level scores for the negative and positive cohorts. **a** Mean anomaly score and standard deviation for positive examinations (future lesion: Yes) and negative examinations (future lesion: No). **b** Swarm plot displaying individual subject scores. The color indicates if one of the studies used to calculate the inter-visit difference image was acquired in Period 1 in which a different protocol and scanner were in use than in Periods 2 and 3, showing that a substantial portion of false positives falls into this category

research to develop corresponding adaptive individualized screening strategies.

Usually, a prophylactic bilateral mastectomy is offered to high-risk women as soon as their risk status has been determined but many women decline surgery at that point [41]. Through dynamic risk profiling the surgery could be offered to women exactly when the risk of cancer development in the following year is even more elevated due to already present anomalies. This would allow a high-risk woman to avoid surgery as long as possible and at the same time prevent her from becoming a cancer patient. A prerequisite for risk adjustment is the identification of precursor appearance signatures at the location of future lesions. A prerequisite for risk adjustment is the identification of precursor appearance signatures at the location of future lesions. Additionally, successful automated detection of anomalies in breast tissue change between subsequent screening visits would save resources for radiologists, who currently have to spend their efforts on visually comparing MRI scans. Despite being time-consuming, a visual comparison is also exhausting and leads to fatigue potentially accompanied with increased susceptibility to reading errors. Reliable automated detection of anomalies could therefore reduce the workload of radiologists and consequently acquire more of their resources for assessing suspicious cases.

Deep learning models have an increasingly important role in the detection and quantification of findings in medical imaging data [18]. The majority of approaches demonstrates that models can be successfully trained by supervision based on large numbers of pairs of available images and labels, such as lesion segmentation [42]. This is feasible for the detection of well-described lesions that can be annotated by experts. However, it does not allow for the discovery of yet unknown predictive signatures in imaging data, since annotation is not possible, or the number of positive subjects is comparably low as is the case in screening scenarios. Anomaly detection approaches such as f-AnoGAN [36] offer to discover anomalies in the change of breast tissue during follow-up, that is linked to future lesion emergence, without the need for extensive annotation for training.

Models based on f-AnoGAN capture complex appearance variability in the negative cohort well and can detect precursor signatures of future lesions without the need for annotation. Previously, GANs have been used for anomaly detection in medical images [36, 43, 44]. In contrast to these results for detecting present lesions, here we use GANs to detect precursor signatures of lesions that have not yet emerged. To our knowledge, this study is the first to propose a GAN-based anomaly detection strategy to predict future lesions in a cohort of high-risk women using CE-MRI scans acquired during screening. We demonstrated that precursor signatures of lesions that emerge at a later time point can be identified by unsupervised machine learning, performing training only on the negative cohort.

Our model, trained on follow-up CE-MRI exams of women at high BC risk who do not develop BC, captures the normal variability of longitudinal change in the appearance of CE-MRI of the breast. Applying this model to new imaging data derives an anomaly score that quantifies the deviation of the observed longitudinal appearance change from normal variability represented in the model. By looking at tissue changes over time, our approach therefore mimics the approach of radiologists when screening images.

In our analysis of cases where the presence of an anomaly misclassified the future emergence of lesions, we identified two primary factors as possible causes. First, the longitudinal dataset collected over a period of 17 years was acquired by a consecutive series of three different scanner parameters. A substantial number of misclassifications were linked to a scanner switch occurring between compared examinations, for various values of the classification threshold T_{exam} for the examination-level score. This suggests unsurprisingly that scanner type and protocol are relevant for an appearance change. In our experiments, the anomaly score was nevertheless an independent predictor for future lesion emergence, with a compromise of sensitivity, specificity, and negative and positive predictive value at $T_{exam} = 0.7$ and $T_{exam} = 0.9$. The second factor that mainly produced false negatives (low anomaly score, despite a lesion emerging at a later time point) was exclusively benign lesions. Classifying BI-RADS 1 or 2 *versus* BI-RADS 3, 4, or 5 therefore showed a raise in sensitivity and negative predictive value. This was, however, also accompanied with a drop of the positive predictive value, mainly caused by false positives that were either related to the scanning period or BI-RADS 2 lesions. The purpose of this study was, however, to predict lesions of any type.

Although the focus of our study is on future lesion prediction, for clinical applicability the preprocessing is also relevant. Twenty-two subjects were removed from the dataset due to unsatisfactory preprocessing results. Registration of follow-up data was to be the least problematic and only one subject was lost due to misregistration of a screening visit acquired during the oldest acquisition period, period 1. Too small breast size for patch extraction affected eight subjects, but was mainly a limitation, for screening visits acquired during Period 2. For scans with higher resolution, such as those in Period 3, only one subject was excluded. A patch size of 64 × 64 might therefore be feasible for most subjects at the resolution of current MRI protocols. Furthermore, the patch size used in the model could be changed, if a smaller patch size should be more feasible. The preprocessing step leading to most exclusions ($n = 13$ subjects) was segmentation, due to unsatisfactory segmentation results. U-nets [42], which are the current state-of-the-art for segmentation, could improve the segmentation of breast tissue. However, they first would need to be trained on already manually annotated MRI scans.

One main limitation of this study is the small sample size with only 64 subjects on the patient level. Apart from that, we evaluated our approach on the patch level, yielding a sample size of 104,531 patches of normal tissue change and 455 patches of future lesion locations. Furthermore, although our method mimics the approach of radiologists when screening imaging data by searching for differences between subsequent screening visits, our model requires at least two consecutive studies reflecting the high-risk screening population, where regular yearly CE-MRI scans of the breast are performed. This makes it inapplicable to women on their first visit. Another limitation of the study is the scanner bias when evaluating our examination-level score. Heterogeneity in medical data, such as the use of different scanners and acquisition protocols, is a common problem for computational image analysis. Nevertheless, our anomaly score was associated with future lesions regardless of this factor. We aggregated BI-RADS 2, 3, 4, or 5 scores to a single class (> BI-RADS 1), without differentiating malignancy. However, we performed a post hoc analysis of the results and investigated the possible malignancy of lesions that were not successfully predicted and found that they were all benign. Even though the study was conducted on 1.5-T CE-MRI data, we expect the results to be transferable directly also to higher field strength scanners such as 3 T. Increased image quality might further facilitate the identification of precursor image signatures.

In summary, anomaly detection is a feasible approach to identify precursor signatures of future lesion emergence in CE-MRI of high-risk women, which might form the basis for adjusting individual screening intervals. Training a representative model of normal variability can detect signatures that are not yet well defined, without the need for annotated examples with lesions. Therefore, our approach is in principle also applicable to CE-MRI of women at normal risk. However, further validation is required to assess the feasibility of implementing corresponding adaptive screening strategies on normal-risk populations. In the context of high-risk screening, the next steps will be the investigation of prediction accuracy for benign and malignant lesions, as well as the influence of background enhancement and breast density on our anomaly score.

Abbreviations

AUC	Area under the curve
BC	Breast cancer
CE-MRI	Contrast-enhanced magnetic resonance imaging
DL	Deep learning
f-AnoGAN	Fast anomaly detection generative adversarial network
GAN	Generative adversarial network
$I_{i,j}^{diff}$	Voxel value difference image of I_i^{sub} and I_j^{sub}
I_i^{sub}	First post-contrast subtraction image of the *i*th available screening visit of a subject
ROC	Receiver operating characteristic

Supplementary Information

The online version contains supplementary material available at https://doi.org/10.1186/s41747-023-00343-y.

Additional file 1.

Acknowledgements

We thank Michael Prinz for helping with the data transfer.

Authors' contributions

BB conducted the experiments presented in this work, created the figures, and was a major contributor to writing the manuscript. MB was a major contributor to writing the manuscript. PS contributed to writing the manuscript. CS collected data in the high-risk breast cancer screening program. GL and TH contributed to the conceptualization of the study and were contributors to the writing and reviewing of the manuscript. The authors read and approved the final manuscript.

Funding

This work was supported by the Medical University of Vienna; by the Comprehensive Cancer Center Forschungsförderung der Initiative Krebsforschung, MedUni Wien; by the Vienna Science and Technology Fund (WWTF) [10.47379/LS20065], [10.47379/LS19018]; by the Austrian Research Fund (FWF, P 35189); by the Anniversary Fund of the Oesterreichische Nationalbank (Nr. 18207) and by the Medical-Scientific Fund of the Mayor of the Federal Capital Vienna (Nr. 20009). This work has received co-funding from the European Union's Horizon Europe research and innovation program under grant agreement No. 101100633-EUCAIM.

Availability of data and materials

The datasets generated and/or analyzed during the current study are not publicly available due to the need for a legal contract regulating data protection but are available from the corresponding author on reasonable request.

Declarations

Ethics approval and consent to participate

This study was conducted in adherence to the tenets of the Declaration of Helsinki, and ethics approval was obtained by the Ethics Committee of the Medical University of Vienna Submission Nr. 461/2003. The study is a prospective data analysis and subjects gave informed consent for inclusion.

Consent for publication

Not applicable.

Competing interests

GL is a co-founder and shareholder of Contextflow GmbH and has received speaking honoraria from Novartis. THH is a member of the ***European Radiology Experimental*** Editorial Board; he has not taken part in the review or selection process of this article. The other authors declare that they have no competing interests.

Author details

[1] Department of Biomedical Imaging and Image-Guided Therapy, Division of Computational Imaging Research (CIR), Medical University of Vienna, Währinger Gürtel 18-20, 1090 Vienna, Austria. [2] Department of Biomedical Imaging and Image-Guided Therapy, Division of General and Pediatric Radiology, Medical University of Vienna, Vienna, Austria. [3] Department of Obstetrics and Gynecology, Division of Special Gynecology, Medical University of Vienna, Vienna, Austria. [4] Comprehensive Cancer Center, Medical University of Vienna, Vienna, Austria. [5] Computer Science and Artificial Intelligence Laboratory, Massachusetts Institute of Technology, Cambridge, MA, USA.

Received: 25 January 2023 Accepted: 4 April 2023
Published online: 07 June 2023

References

1. Ferlay J, Colombet M, Soerjomataram I et al (2019) Estimating the global cancer incidence and mortality in 2018: GLOBOCAN sources and methods. Int J Cancer 144:1941–1953. https://doi.org/10.1002/ijc.31937
2. Domchek SM, Friebel TM, Neuhausen SL et al (2006) Mortality after bilateral salpingo-oophorectomy in BRCA1 and BRCA2 mutation carriers: a prospective cohort study. Lancet Oncol 7:223–229
3. Ludwig KK, Neuner J, Butler A et al (2016) Risk reduction and survival benefit of prophylactic surgery in BRCA mutation carriers, a systematic review. Am J Surg 212:660–669. https://doi.org/10.1016/j.amjsurg.2016.06.010
4. Phi X-A, Saadatmand S, De Bock GH et al (2016) Contribution of mammography to MRI screening in BRCA mutation carriers by BRCA status and age: individual patient data meta-analysis. Br J Cancer 114:631–637. https://doi.org/10.1038/bjc.2016.32
5. Lee CS, Monticciolo DL, Moy L (2020) Screening guidelines update for average-risk and high-risk women. AJR Am J Roentgenol 214:316–323. https://doi.org/10.2214/AJR.19.22205
6. Singer CF, Tea M-K, Pristauz G et al (2012) Guideline for the prevention and early detection of breast and ovarian cancer in high risk patients, particularly in women from HBOC (hereditary breast and ovarian cancer) families. Wien Klin Wochenschr 124:334–339. https://doi.org/10.1007/s00508-012-0173-6
7. Marino MA, Riedl CC, Bernathova M et al (2018) Imaging phenotypes in women at high risk for breast cancer on mammography, ultrasound, and magnetic resonance imaging using the fifth edition of the Breast Imaging Reporting and Data System. Eur J Radiol 106:150–159. https://doi.org/10.1016/j.ejrad.2018.07.026
8. Kim G, Bahl M (2021) Assessing risk of breast cancer: a review of risk prediction models. J Breast Imaging 3:144–155
9. Passaperuma K, Warner E, Causer PA et al (2012) Long-term results of screening with magnetic resonance imaging in women with BRCA mutations. Br J Cancer 107:24–30
10. Phi X-A, Houssami N, Hooning MJ et al (2017) Accuracy of screening women at familial risk of breast cancer without a known gene mutation: individual patient data meta-analysis. Eur J Cancer 85:31–38. https://doi.org/10.1016/j.ejca.2017.07.055
11. Vreemann S, Gubern-Merida A, Lardenoije S et al (2018) The frequency of missed breast cancers in women participating in a high-risk MRI screening program. Breast Cancer Res Treat 169:323–331
12. Yamaguchi K, Schacht D, Newstead GM et al (2013) Breast cancer detected on an incident (second or subsequent) round of screening MRI:

MRI features of false-negative cases. AJR Am J Roentgenol 201:1155–1163. https://doi.org/10.2214/AJR.12.9707

13. Pages EB, Millet I, Hoa D et al (2012) Undiagnosed breast cancer at MR imaging: analysis of causes. Radiology 264:40–50. https://doi.org/10.1148/radiol.12111917
14 Yala A, Mikhael PG, Strand F et al (2021) Toward robust mammography-based models for breast cancer risk. Sci Transl Med 13:eaba4373. https://doi.org/10.1126/scitranslmed.aba4373
15. Yala A, Lehman C, Schuster T et al (2019) A deep learning mammography-based model for improved breast cancer risk prediction. Radiology 292:60–66. https://doi.org/10.1148/radiol.2019182716
16. Dembrower K, Liu Y, Azizpour H et al (2020) Comparison of a deep learning risk score and standard mammographic density score for breast cancer risk prediction. Radiology 294:265–272. https://doi.org/10.1148/radiol.2019190872
17. Clift AK, Dodwell D, Lord S et al (2021) The current status of risk-stratified breast screening. Br J Cancer 126:533–550. https://doi.org/10.1038/s41416-021-01550-3
18. McBee MP, Awan OA, Colucci AT et al (2018) Deep learning in radiology. Acad Radiol 25:1472–1480. https://doi.org/10.1016/j.acra.2018.02.018
19. Rowlands CF, Baralle D, Ellingford JM (2019) Machine learning approaches for the prioritization of genomic variants impacting pre-mRNA splicing. Cells 8:1513
20. Lehman CD, Wellman RD, Buist DSM et al (2015) Diagnostic accuracy of digital screening mammography with and without computer-aided detection. JAMA Intern Med 175:1828
21. Dalmış MU, Gubern-Mérida A, Vreemann S et al (2016) A computer-aided diagnosis system for breast DCE-MRI at high spatiotemporal resolution. Med Phys 43:84. https://doi.org/10.1118/1.4937787
22. Meyer-Bäse A, Morra L, Meyer-Bäse U, Pinker K (2020) Current status and future perspectives of artificial intelligence in magnetic resonance breast imaging. Contrast Media Mol Imaging 2020:6805710. https://doi.org/10.1155/2020/6805710
23. Herent P, Schmauch B, Jehanno P et al (2019) Detection and characterization of MRI breast lesions using deep learning. Diagn Interv Imaging 100:219–225. https://doi.org/10.1016/j.diii.2019.02.008
24. Dalmış MU, Vreemann S, Kooi T et al (2018) Fully automated detection of breast cancer in screening MRI using convolutional neural networks. J Med Imaging (Bellingham) 5:014502. https://doi.org/10.1117/1.JMI.5.1.014502
25. Lu W, Wang Z, He Y, et al (2019) Breast cancer detection based on merging four modes MRI using convolutional neural networks. In: ICASSP 2019 - 2019 IEEE International Conference on Acoustics, Speech and Signal Processing (ICASSP), Brighton, UK, 2019, pp. 1035–1039. https://doi.org/10.1109/ICASSP.2019.8683149
26. Rodriguez-Ruiz A, Lång K, Gubern-Merida A et al (2019) Can we reduce the workload of mammographic screening by automatic identification of normal exams with artificial intelligence? A feasibility study. Eur Radiol 29:4825–4832. https://doi.org/10.1007/s00330-019-06186-9
27. Yala A, Schuster T, Miles R et al (2019) A deep learning model to triage screening mammograms: a simulation study. Radiology 293:38–46. https://doi.org/10.1148/radiol.2019182908
28. Xu Y, Hosny A, Zeleznik R et al (2019) Deep learning predicts lung cancer treatment response from serial medical imaging. Clin Cancer Res 25:3266–3275. https://doi.org/10.1158/1078-0432.CCR-18-2495
29. Abdullah Alfayez A, Kunz H, Grace Lai A (2021) Predicting the risk of cancer in adults using supervised machine learning: a scoping review. BMJ Open 11:e047755. https://doi.org/10.1136/bmjopen-2020-047755
30. Lu MT, Raghu VK, Mayrhofer T et al (2020) Deep learning using chest radiographs to identify high-risk smokers for lung cancer screening computed tomography: development and validation of a prediction model. Ann Intern Med 173:704–713. https://doi.org/10.7326/M20-1868
31. Riedl CC, Luft N, Bernhart C et al (2015) Triple-modality screening trial for familial breast cancer underlines the importance of magnetic resonance imaging and questions the role of mammography and ultrasound regardless of patient mutation status, age, and breast density. J Clin Oncol 33:1128–1135. https://doi.org/10.1200/JCO.2014.56.8626
32. Riedl CC, Ponhold L, Flöry D et al (2007) Magnetic resonance imaging of the breast improves detection of invasive cancer, preinvasive cancer, and premalignant lesions during surveillance of women at high risk for breast cancer. Clin Cancer Res 13:6144–6152. https://doi.org/10.1158/1078-0432.CCR-07-1270
33. Milos RI, Pipan F, Kalovidouri A et al (2020) The Kaiser score reliably excludes malignancy in benign contrast-enhancing lesions classified as BI-RADS 4 on breast MRI high-risk screening exams. Eur Radiol 30:6052–6061. https://doi.org/10.1007/s00330-020-06945-z
34. Yushkevich PA, Piven J, Hazlett HC et al (2006) User-guided 3D active contour segmentation of anatomical structures: significantly improved efficiency and reliability. Neuroimage 31:1116–1128
35 American College of Radiology (2003) Breast Imaging and Reporting Data System (BI-RADS) Atlas. American College of Radiology, Reston
36. Schlegl T, Seeböck P, Waldstein SM et al (2019) f-AnoGAN: fast unsupervised anomaly detection with generative adversarial networks. Med Image Anal 54:30–44. https://doi.org/10.1016/j.media.2019.01.010
37. Burger B, Bernathova M, Helbich T, Singer CF, Langs G (2020) "AI-based prediction of lesion occurrence in high-risk women based on anomalies detected in follow-up examinations," Proc. SPIE 11513, 15th International Workshop on Breast Imaging (IWBI2020), 115130P. https://doi.org/10.1117/12.2564313
38. Arjovsky, M., Chintala, S., and Bottou, L. Wasserstein GAN. arXiv:1701.07875v3
39. Efron B (1992) Bootstrap methods: another look at the jackknife. In: Kotz S, Johnson NL (eds) Breakthroughs in Statistics. Springer Series in Statistics. Springer, New York. https://doi.org/10.1007/978-1-4612-4380-9_41
40. Fluss R, Faraggi D, Reiser B (2005) Estimation of the Youden Index and its associated cutoff point. Biom J 47:458–472. https://doi.org/10.1002/bimj.200410135
41. Grann VR, Jacobson JS, Sundararajan V et al (1999) The quality of life associated with prophylactic treatments for women with BRCA1/2 mutations. Cancer J Sci Am 5:283–292
42. Ronneberger O, Fischer P, Brox T (2015) U-Net: Convolutional networks for biomedical image segmentation. In: Navab N, Hornegger J, Wells W, Frangi A (eds) Medical image computing and computer-assisted intervention – MICCAI 2015. MICCAI 2015. Lecture Notes in Computer Science, vol 9351. Springer, Cham. https://doi.org/10.1007/978-3-319-24574-4_28
43. Fujioka T, Kubota K, Mori M et al (2020) Efficient anomaly detection with generative adversarial network for breast ultrasound imaging. Diagnostics (Basel) 10:456. https://doi.org/10.3390/diagnostics10070456
44. Swiecicki A, Konz N, Buda M, Mazurowski MA (2021) A generative adversarial network-based abnormality detection using only normal images for model training with application to digital breast tomosynthesis. Sci Rep 11:10276. https://doi.org/10.1038/s41598-021-89626-1

Publisher's Note

Springer Nature remains neutral with regard to jurisdictional claims in published maps and institutional affiliations.